HHS Public Access

Author manuscript

Angew Chem Int Ed Engl. Author manuscript; available in PMC 2020 August 05.

Published in final edited form as:

Angew Chem Int Ed Engl. 2019 August 05; 58(32): 10936–10940. doi:10.1002/anie.201904672.

Direct Resonance Raman Characterization of a Peroxynitrito Copper Complex Generated from O_2 and NO and Mechanistic Insights into Metal Mediated Peroxynitrite Decomposition

Jeffrey J. Liu[a], **Maxime A. Siegler**[a], **Kenneth D. Karlin**[*,a], **Pierre Moënne-Loccoz**[*,b]

[a]Department of Chemistry, Johns Hopkins University, Baltimore, MD 21218 (USA)

[b]Department of Biochemistry and Molecular Biology, Oregon Health & Science University, Portland, OR 97239 (USA)

Abstract

We report the formation of a new copper peroxynitrite (**PN**) complex $[Cu^{II}(TMG_3tren)(\kappa^1\text{-}OONO)]^+$ (**PN1**) from reaction of $[Cu^{II}(TMG_3tren)(O_2^{\bullet-})]^+$ (**1**) with $NO^{\bullet}_{(g)}$ at –125 °C. The first resonance Raman spectroscopic characterization of such a metal bound **PN** moiety supports a *cis* κ^1-$OONO^-$ geometry. **PN1** transforms thermally to an isomeric form (**PN2**) with κ^2-O,O'-($^-$OONO) coordination, which undergoes O–O bond homolysis to generate a putative cupryl ($LCu^{II}–O^{\bullet}$) intermediate and $NO_2^{\bullet}$. These transient species do not recombine to give a nitrato (NO_3^-) product but instead proceed to effect oxidative chemistry and formation of a Cu(II)-nitrito (NO_2^-) complex (**2**).

Graphical Abstract

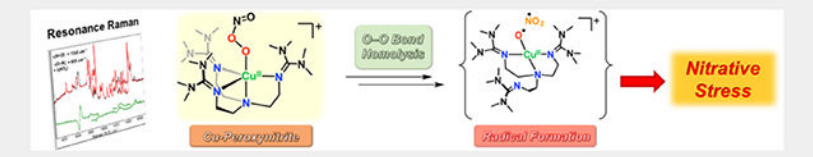

Keywords

Bioinorganic Chemistry; Copper; Nitrogen Oxides; Raman Spectroscopy; Peroxynitrite

Nitric oxide ($NO^{\bullet}$) is an essential molecule in biology due to its role as a signaling agent,[1–3] its utilization in the human immune response,[4–6] and as an obligatory intermediate in the geobiochemical nitrogen cycle.[7,8] At elevated concentrations (μM) $NO^{\bullet}$ is toxic[4,9–12] and its downstream derivatives can lead to oxidation and nitration of proteins[13–15], lipids[16,17] and nucleic acids.[18,19] Phagocytes leverage the toxicity of nitric oxide in combination with other reactive nitrogen and oxygen species (such as $O_2^{\bullet-}$, H_2O_2 and NO_2^-) as tools to combat invading microorganisms.[5,6] Phagocytes also employ metal toxicity, and

* karlin@jhu.edu, moennelo@ohsu.edu.

Supporting information for this article is given via a link at the end of the document.

in particular copper, as a bactericide, but the synergy between destructive reactive nitrogen and oxygen species and copper burst in the macrophage remains largely unknown.[6,20–22] A key intermediate postulated to be responsible for nitric oxide's toxicity is peroxynitrite ($^-$OONO, **PN**), which may be derived from NO$^\bullet$ and $O_2^{\bullet-}$ (Scheme 1).[23–25] Peroxynitrite can exist in two isomers, *cis*, or *trans*, and upon protonation, or in the presence of CO_2, yield either nitrate, or freely diffusing radicals such as $NO_2^\bullet$, HO$^\bullet$, and $CO_3^{\bullet-}$.[10,26] Studies of aqueous peroxynitrite have deduced that the predominant decay pathway is isomerization to nitrate.[27,28]

Metal coordinated peroxynitrites are of interest due to the intimate role metals play in the regulation and processing of both NO$^\bullet$ and $O_2^{\bullet-}$,[3,29–32] which may implicate metals as important factors in the physiological formation and transformations of peroxynitrite (Scheme 1). While progress has been made to implicate metal ions in the decay of peroxynitrite, a discrete peroxynitrite coordination complex is rarely observed.[33–42] Examples of stable peroxynitrite complexes are scarce[43,44], and those containing vibrational (i.e., IR spectroscopic) information about the peroxynitrite ligand even more so.[45–48]

In a previous report we have described the formation of a cupric-peroxynitrite complex from the addition of NO$^\bullet$ to $[Cu^{II}(TMG_3tren)(O_2^{\bullet-})]^+$ (**1**) at –80 ºC to generate the cupric-peroxynitrito complex $[Cu^{II}(TMG_3tren)(\kappa^2\text{-O,O'-OONO})]^+$ (**PN2**) (Scheme 2).[49] Direct vibrational evidence of this peroxynitrite complex was unable to be obtained, and information concerning the structural identity was derived from EPR spectroscopy and density functional theory (DFT) calculations. Herein we report the formation of a new peroxynitrite complex, $[Cu^{II}(TMG_3tren)(\kappa^1\text{-OONO})]^+$ (**PN1**) formed prior to **PN2**, and the resonance Raman (RR) spectroscopic characterization of **PN1** which to our knowledge is the first RR characterization of a metal-peroxynitrite species.

The complex **PN1** is generated from the addition of NO$^\bullet$ solubilized in 2-methyltetrahydrofuran ($NO_{(MeTHF)}$, see SI), to **1** at –125 ºC (Scheme 2). Monitoring the reaction by UV-vis spectroscopy reveals the gradual decrease of the cupric-superoxide features at 448, 679 and 791 nm and accompanied by the appearance of a new intense electronic transition at 310 nm (7300 M^{-1} cm^{-1}) and a weak d-d transition at 1000 nm (~410 M^{-1} cm^{-1}) (Figure 1). The intense high-energy feature near 310 nm has been has been reported for alkali and ammonium salts[50,51] and in metal coordination complexes of peroxynitrite.[43,45]

Formation of **PN1** is easily monitored via EPR spectroscopy. Addition of $NO_{(MeTHF)}$ to the EPR silent **1** leads to the generation of an active EPR signal (Figure 2), consistent with the radical coupling of **1** (S = 1)[52] with NO$^\bullet$ (S = ½) to give a S = ½ complex. A quantitative analysis of the EPR data through a Job's plot shows maximal **PN1** formation at a 1:1 mole ratio of Cu to NO$^\bullet$, confirming the 1:1 cupric-superoxide to NO stoichiometry (Figure S1).

The RR spectra of **PN1** reveal multiple isotopically sensitive features assigned to stretching and bending modes of the cupric-peroxynitrite complex (Figure 3). The feature with the highest intensity is at 658 cm^{-1} and shows a 30 cm^{-1} downshift with full labeling of the

peroxynitrite ligand (i.e., $^{18}O^{18}O^{15}N^{18}O$). This RR signal is unusually broad with a 29 cm^{-1} full width at half maximum (FWHM), and is reminiscent of the broad 642 cm^{-1} band observed in the Raman spectrum of the *cis* peroxynitrite anion in aqueous solution.[53,54] Labeling with $^{18}O_2$ or $^{15}N^{18}O$ shifts the 658 cm^{-1} band –26 and –9 cm^{-1} respectively, supporting significant O–N stretching character to this mode which was otherwise assigned to an out of plane deformation in the free ion (Table 1 and Figure S2). Indeed, the observed shifts match well calculated shifts based on Hooke's law for an O–N oscillator (–29.5 cm^{-1} with ^{18}O–^{15}N, –17 cm^{-1} with ^{18}O–N, and –12 cm^{-1} with O–^{15}N). The DFT vibrational analysis also supports a mode description that combines O–N stretch with O-ON=O bending (see below).

A much weaker and sharper band at 1545 cm^{-1} band is readily assigned to the peroxynitrite ν(N=O) stretch based on its frequency and large downshift with $^{15}N^{18}O$ (–65 cm^{-1}) (Figure 3). This assignment is further strengthened by the limited sensitivity of this mode to the labeling of O_2 ($\Delta^{18}O_2$ = –2 cm^{-1}) (Table 1 and Figure S3).

A band at 929 cm^{-1} strongly impacted by O_2 labeling ($\Delta^{18}O_2$ = –29 cm^{-1}) as well as NO labeling ($\Delta^{15}N^{18}O$ = –17 cm^{-1}) is assigned to an O–O stretch mixed with an O-N=O bend (Table 1 and Figure S4). A very weak band at 812 cm^{-1}, which can be extracted from the MeTHF Raman spectrum background only after labeling of both O_2 and NO, is tentatively assigned to another mixed vibrational mode that combines O–O stretch with in plane OO-N=O deformation. Finally, a broad signal at 1282 cm^{-1} that shifts –60 cm^{-1} after full labeling of the peroxynitrito group and that shows a moderate intensity relative to the fundamental mode at 658 cm^{-1} is likely to correspond to its first overtone.[55]

To aid interpretation of the RR data, predicted structures for **PN1** were obtained via DFT calculations. The reverse axial copper EPR signal (Figure 2) is indicative of a trigonal bipyramidal copper geometry. Based on that constraint two possible structures were calculated, where the peroxynitrite ligand in either a *cis* or *trans* confirmation (Figures S5 & S6). The *cis* cupric-peroxynitrite isomer is predicted to be the more stable isomer by 4.1 kcal/mol, in line with previously reported calculations of the anion where the *cis* isomer is more stable by 3 kcal/mol.[53] The calculated Raman spectra provide satisfactory match with the experimental data, with the most highly Raman-active vibration observed in the mid-frequency range with significant O–N stretching character (Figures S7–S9). Calculated frequencies for this mode are 708 cm^{-1} in the *cis*-**PN** and 845 cm^{-1} in the *trans*-**PN** conformer, the former matching better with the 658 cm^{-1} observed frequency. Similarly, the calculated frequencies for modes dominated by ν(O–O) and ν(N=O) for the *cis*-**PN** are better match than that of the *trans*-**PN** (Table 1). In fact, the four fundamental Raman frequencies observed in **PN1** are reproduced in the calculated spectrum of *cis*-PN with overestimations ranging from 0.02 to 0.08 typical of DFT calculations. Thus, the RR data support a *cis* geometry for the peroxynitrite ligand in **PN1**, as depicted in Scheme 2.

When $NO^{\bullet}$ is added to **1** at –80 ºC a chelating peroxynitrite intermediate $[Cu^{II}(TMG_3tren)(\kappa^2\text{-O,O'-OONO})]^+$ (**PN2**) is formed, giving an axial EPR spectrum;[49] as described above, **PN1** is formed at –125 ºC exhibiting a reverse axial copper geometry (Figure S10). If $NO^{\bullet}$ is added at an intermediate temperature (–98 ºC) **PN1** is observed as the initial species

followed by conversion to **PN2.** The conversion from reverse axial to axial EPR signal (Figure 4) reflects a change in the copper center geometry from trigonal bipyramidal to square pyramidal. Such a change results in the deligation one of the tetramethylguanidine (TMG) arms which allows for the adaptation of a square pyramidal geometry.[49] Careful analysis of the EPR spectra after 60 minutes reveal the presence of two axial Cu signals (Figure 4) which is assigned to the partial decomposition of **PN2** to the final Cu-nitrito product (see below).

Attempts to obtain RR spectra from **PN2** were inconclusive. Gradual photo-bleaching of **PN1** was observed during the acquisition of the Raman spectra and presumably **PN2** exhibits a greater photosensitivity.

Upon further warming to –60 ºC, **PN2** decays to a chelating copper nitrito species $[Cu^{II}(TMG_3tren)(\kappa^2\text{-}O,O'\text{-}NO_2)]^+$ (**2**) confirmed by ESI–MS (Figure S11). EPR spectroscopy (Figure S12) indicates the copper maintains a tetragonal coordination geometry, thus also with one deligated ligand arm, as confirmed by comparison of UV-vis and EPR properties with a square-pyramidal $Cu^{II}\text{-}NO_2^-$ analogue with tridentate ligand, $[Cu^{II}(TMG_2dien)k^2\text{-}O,O'\text{-}NO_2^-)]^+$ (X-ray structure, UV-vis & EPR properties have also been determined; Figures S13 and S14). UV-vis quantification puts the yield of **2** at 95 ± 4% (Figure S15), and the presence of nitrite was independently quantified via a Griess assay was found to be in good yield (75 ± 2 %) (Figure S16 & Table S1). The kinetics of **PN2** transformation to $Cu^{II}\text{-}NO_2$ species **2** indicated overall first order in Cu behavior (Figure S17) consistent with unimolecular decay, most likely though cleavage of the O–O bond. This result rules against higher order copper adducts participating in peroxynitrite decay as suggested in the aqueous H^+ and CO_2 mediated decay pathways.[27,28]

The detection and characterization (see SI) of a high yield cupric-nitrite (NO_2^-) product from **PN2** thermal transformation is consistent with the formation of cupryl $[Cu^{II}(TMG_3tren)(O^\bullet)]^+$ and $NO_2^\bullet$ intermediates following peroxynitrite homolytic O–O bond cleavage; the most common recombination of such radicals to give a Cu-nitrate product does not occur (Scheme 1). In the absence of substrate we postulate the putative cupryl intermediate goes on to hydroxylate the solvent via a radical rebound pathway to give LCu^I and R–OH (R = solvent) before LCu^I reacts with $NO_2^\bullet$ to yield $LCu^{II}\text{–}(NO_2^-)$ as the final product (Scheme S1).[36,44,46,56,57] To verify the generation of these radical species, addition of >500 equiv excess of 2,4-di-*tert*-butylphenol (DTBP) results in the nearly quantitative formation of both **2** and the coupled bis-phenol product, 3,3',5,5'-tetra-*tert*-butyl-[1,1'-biphenyl]-2,2'-diol (Figures S18 & S19). The coupling of phenoxyl species to give the observed diol can be rationalized by successive hydrogen atom abstractions by $LCu^{II}\text{–}O^\bullet$ and $NO_2^\bullet$ (a strong oxidant[58,59]) to give LCu^{II}–OH and HNO_2 before ligand exchange to give $LCu^{II}\text{–}NO_2$ and H_2O (Scheme 3). A concerted O–O bond cleavage / O–H bond activation pathway is also plausible; further mechanistic studies will be required to differentiate between stepwise and concerted substrate oxidation. Additional experiments using 5,5-dimethyl-1-pyrroline *N*-oxide (DMPO, 500 equiv), a known radical trapping agent used to probe O–O bond scission reactions,[60,61] resulted in detection of LCu^{II}(O–DMPO) by ESI-MS (Figure S20) following warming of the reaction mixture. These results are

consistent with the generation of two equivalents of oxidant per equivalent of copper-peroxynitrite, the two species deriving from O-O bond cleavage.

In summary, we have described the synthesis and preparation of the first transition metal-peroxynitrite complex characterized by resonance Raman spectroscopy. Comparison with Raman data from alkylammonium *cis*-peroxynitrite, combined with analytical Raman calculations have suggested the peroxynitrito ligand is coordinated to copper in a *cis*-geometry. Thermal transformation of this peroxynitrite complex leads to O–O homolysis and the generation of LCu–$O^{\bullet}$ and $NO_2^{\bullet}$ which go on to perform further oxidative chemistry. These results further underscore the importance of understanding the biological role transition metal ions may play in biochemical oxidative and nitrative damage.

Supplementary Material

Refer to Web version on PubMed Central for supplementary material.

Acknowledgements

This work was supported by the National Institutes of Health (NIH) (GM28962 to K.D.K. and GM074785 to P.M.-L.). J.J.L. thanks the Zeltmann family for the Eugene W. and Susan C. Zeltmann fellowship.

References

[1]. Ignarro LJ, Annu. Rev. Pharmacol. Toxicol 1990, 30, 535–560. [PubMed: 2188578]

[2]. Ignarro LJ, Nitric Oxide as a Communication Signal in Vascular and Neuronal Cells, Academic Press, San Diego, 1996.

[3]. Tennyson AG, Lippard SJ, Chem. Biol 2011, 18, 1211–1220. [PubMed: 22035790]

[4]. Toledo JC, Augusto O, Chem. Res. Toxicol 2012, 25, 975–989. [PubMed: 22449080]

[5]. Hu K, Li Y, Rotenberg SA, Amatore C, Mirkin MV, J. Am. Chem. Soc 2019, 141, 4564–4568. [PubMed: 30827109]

[6]. Dalecki AG, Crawford CL, Wolschendorf F, in Adv. Microb. Physiol. (Ed.: Poole RK), Elsevier Ltd, Oxford, UK, 2017, pp. 193–260.

[7]. Lehnert N, Dong HT, Harland JB, Hunt AP, White CJ, Nat. Rev. Chem 2018, 2, 278–289.

[8]. Lancaster KM, Caranto JD, Majer SH, Smith MA, Joule 2018, 2, 421–441.

[9]. Pacher P, Beckman JS, Liaudet L, Physiol. Rev 2007, 87, 315–424. [PubMed: 17237348]

[10]. Ferrer-Sueta G, Campolo N, Trujillo M, Bartesaghi S, Carballal S, Romero N, Alvarez B, Radi R, Chem. Rev 2018, 118, 1338–1408. [PubMed: 29400454]

[11]. Radi R, Proc. Natl. Acad. Sci. U. S. A 2018, 115, 5839–5848. [PubMed: 29802228]

[12]. Li Y, Hu K, Yu Y, Rotenberg SA, Amatore C, Mirkin MV, J. Am. Chem. Soc 2017, 139, 13055–13062. [PubMed: 28845981]

[13]. Ischiropoulos H, Zhu L, Chen J, Tsai M, Martin JC, Smith CD, Beckman JS, Arch. Biochem. Biophys 1992, 298, 431–7. [PubMed: 1416974]

[14]. Demicheli V, Moreno DM, Jara GE, Lima A, Carballal S, Ríos N, Batthyany C, Ferrer-Sueta G, Quijano C, EstrÍn DA, et al., Biochemistry 2016, 55, 3403–3417. [PubMed: 27227512]

[15]. Ye H, Li H, Gao Z, Chem. Res. Toxicol 2018, 31, 904–913. [PubMed: 30079723]

[16]. Jain K, Siddam A, Marathi A, Roy U, Falck JR, Balazy M, Free Radic. Biol. Med 2008, 45, 269–283. [PubMed: 18457679]

[17]. Davies SS, Guo L, in Mol. Basis Oxidative Stress, John Wiley & Sons, Inc., Hoboken, NJ, USA, 2013, pp. 49–70.

[18]. Fujii S, Sawa T, Ihara H, Tong KI, Ida T, Okamoto T, Ahtesham AK, Ishima Y, Motohashi H, Yamamoto M, et al., J. Biol. Chem 2010, 285, 23970–23984. [PubMed: 20498371]

[19]. Ahmed KA, Sawa T, Ihara H, Kasamatsu S, Yoshitake J, Rahaman MM, Okamoto T, Fujii S, Akaike T, Biochem. J 2012, 441, 719–730. [PubMed: 21967515]

[20]. White C, Lee J, Kambe T, Fritsche K, Petris MJ, J. Biol. Chem 2009, 284, 33949–33956. [PubMed: 19808669]

[21]. Achard MES, Stafford SL, Bokil NJ, Chartres J, Bernhardt PV, Schembri MA, Sweet MJ, McEwan AG, Biochem. J 2012, 444, 51–57. [PubMed: 22369063]

[22]. Fu Y, Chang F-MJ, Giedroc DP, Acc. Chem. Res 2014, 47, 3605–3613. [PubMed: 25310275]

[23]. Beckman JS, in Nitric Oxide Princ. Actions (Ed.: Lancaster JJ), Academic Press, Inc, San Diego, 1996, pp. 1–82.

[24]. Blough NV, Zafiriou OC, Inorg. Chem 1985, 24, 3502–3504.

[25]. Bohle DS, Curr. Opin. Chem. Biol 1998, 2, 194–200. [PubMed: 9667929]

[26]. Goldstein S, Merényi G, in Methods Enzymol, 2008, pp. 49–61. [PubMed: 18237627]

[27]. Molina C, Kissner R, Koppenol WH, Dalton Trans. 2013, 42, 9898–9905. [PubMed: 23698514]

[28]. Serrano-Luginbuehl S, Kissner R, Koppenol WH, Chem. Res. Toxicol 2018, 31, 721–730. [PubMed: 30040390]

[29]. Sheng Y, Abreu IA, Cabelli DE, Maroney MJ, Miller AF, Teixeira M, Valentine JS, Chem. Rev 2014, 114, 3854–3918. [PubMed: 24684599]

[30]. Herold S, Koppenol WH, Coord. Chem. Rev 2005, 249, 499–506.

[31]. Schopfer MP, Wang J, Karlin KD, Inorg. Chem 2010, 49, 6267–6282. [PubMed: 20666386]

[32]. Su J, Groves JT, Inorg. Chem 2010, 49, 6317–6329. [PubMed: 20666389]

[33]. Koebke KJ, Pauly DJ, Lerner L, Liu X, Pacheco AA, Inorg. Chem 2013, 52, 7623–7632. [PubMed: 23768169]

[34]. Gogoi K, Saha S, Mondal B, Deka H, Ghosh S, Mondal B, Inorg. Chem 2017, 56, 14438–14445. [PubMed: 29131596]

[35]. Yokoyama A, Cho K-B, Karlin KD, Nam W, J. Am. Chem. Soc 2013, 135, 14900–14903. [PubMed: 24066924]

[36]. Kumar P, Lee Y, Hu L, Chen JJ, Jun Y, Yao J, Chen H, Karlin KD, Nam W, Park YJ, et al., J. Am. Chem. Soc 2016, 138, 7753–7762. [PubMed: 27221953]

[37]. Hong S, Kumar P, Bin Cho K, Lee YM, Karlin KD, Nam W, Angew. Chemie - Int. Ed 2016, 55, 12403–12407.

[38]. Kurtikyan TS, Ford PC, Chem. Commun 2010, 46, 8570–8572.

[39]. Schopfer MP, Mondal B, Lee D, Sarjeant AAN, Karlin KD, J. Am. Chem. Soc 2009, 131, 11304–11305. [PubMed: 19627146]

[40]. Kalita A, Kumar P, Mondal B, Chem. Commun 2012, 48, 4636–4638.

[41]. Kalita A, Deka RC, Mondal B, Inorg. Chem 2013, 52, 10897–903. [PubMed: 24059697]

[42]. Mondal B, Saha S, Borah D, Mazumdar R, Mondal B, Inorg. Chem 2019, 58, 1234–1240. [PubMed: 30623661]

[43]. Park GY, Deepalatha S, Puiu SC, Lee D-H, Mondal B, Narducci Sarjeant AA, del Rio D, Pau MYM, Solomon EI, Karlin KD, J. Biol. Inorg. Chem 2009, 14, 1301–11. [PubMed: 19662443]

[44]. Sharma SK, Schaefer AW, Lim H, Matsumura H, Moënne-Loccoz P, Hedman B, Hodgson KO, Solomon EI, Karlin KD, J. Am. Chem. Soc 2017, 139, 17421–17430. [PubMed: 29091732]

[45]. Wick PK, Kissner R, Koppenol WH, Helv. Chim. Acta 2000, 83, 748–754.

[46]. Kurtikyan TS, Eksuzyan SR, Hayrapetyan VA, Martirosyan GG, Hovhannisyan GS, Goodwin JA, J. Am. Chem. Soc 2012, 134, 13861–70. [PubMed: 22881578]

[47]. Kurtikyan TS, Eksuzyan SR, Goodwin JA, Hovhannisyan GS, Inorg. Chem 2013, 52, 12046–56. [PubMed: 24090349]

[48]. Cao R, Elrod LT, Lehane RL, Kim E, Karlin KD, J. Am. Chem. Soc 2016, 138, 16148–16158. [PubMed: 27960334]

[49]. Maiti D, Lee D-H, Narducci Sarjeant AA, Pau MYM, Solomon EI, Gaoutchenova K, Sundermeyer J, Karlin KD, J. Am. Chem. Soc 2008, 130, 6700–6701. [PubMed: 18457392]

[50]. Bohle DS, Glassbrenner PA, Hansert B, in Methods Enzymol, 1996, pp. 302–311.

[51]. Lo W, Lee Y, Tsai JM, Beckman S, Chem. Phys. Lett 1995, 242, 147–152.

[52]. Woertink JS, Tian L, Maiti D, Lucas HR, Himes R. a, Karlin KD, Neese F, Würtele C, Holthausen MC, Bill E, et al., Inorg. Chem 2010, 49, 9450–9. [PubMed: 20857998]

[53]. Tsai JM, Harrison JJG, Martin JC, Hamilton TP, Van Der Woerd M, Jablonsky MJ, Beckman JS, J. Am. Chem. Soc 1994, 116, 4115–4116.

[54]. Tsai H, Hamilton TP, Tsai JM, Van Der Woerd M, Harrison JG, Jablonsky MJ, Beckman JS, Koppenol WH, J. Phys. Chem 1996, 100, 15087–15095.

[55]. Calculating the anharmonicity constant based on these two observed Raman frequencies leads to a frequency corrected for anharmonicity of 692 cm–1 well matched by the DFT frequency calculations for the cis-PN1 optimized geometry.

[56]. Kalita A, Kumar P, Mondal B, Chem. Commun 2012, 48, 4636–4638.

[57]. Unlike a previous report using the same system where a putative cupryl (generated via O2 and H-atom donor or directly via an O-atom donor) performs intramolecular hydroxylation,[62] no such reaction takes place in the present study as evidenced by ESI-MS.

[58]. Wilmarth WK, Stanbury DM, Byrd JE, Po HN, Chua C, Coord. Chem. Rev 1983, 51, 155–179.

[59]. Koppenol WH, Moreno JJ, Pryor WA, Ischiropoulos H, Beckman JS, Chem. Res. Toxicol 1992, 5, 834–842. [PubMed: 1336991]

[60]. Kunishita A, Ishimaru H, Nakashima S, Ogura T, Itoh S, J. Am. Chem. Soc 2008, 130, 4244–4245. [PubMed: 18335943]

[61]. Iovan DA, Wrobel AT, McClelland AA, Scharf AB, Edouard GA, Betley TA, Chem. Commun 2017, 53, 10306–10309.

[62]. Maiti D, Lee D-H, Gaoutchenova K, Würtele C, Holthausen MC, Narducci Sarjeant AA, Sundermeyer J, Schindler S, Karlin KD, Angew. Chemie Int. Ed 2008, 47, 82–85.

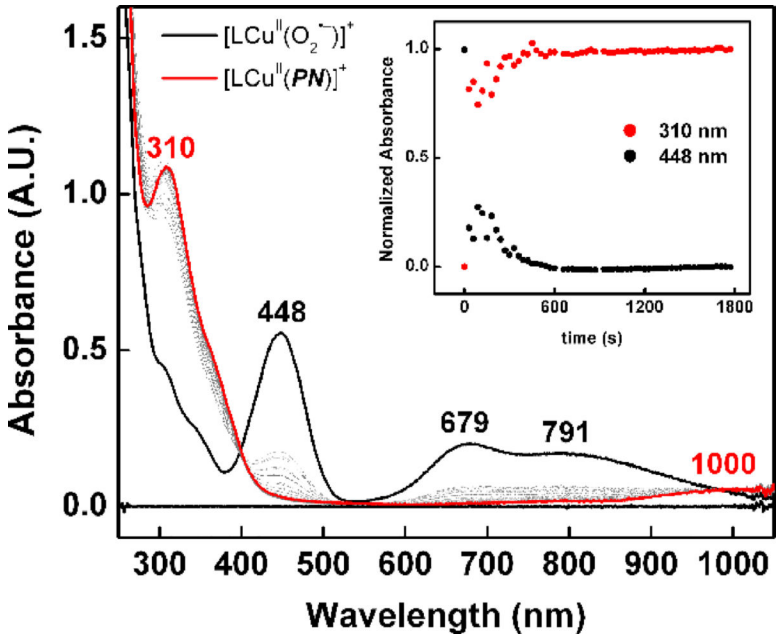

Figure 1.

Addition of $NO_{(MeTHF)}$ (7 equiv) to **1** (0.15 mM) in MeTHF at –125 ºC (black); full conversion to **PN1** was observed within 30 minutes (red).

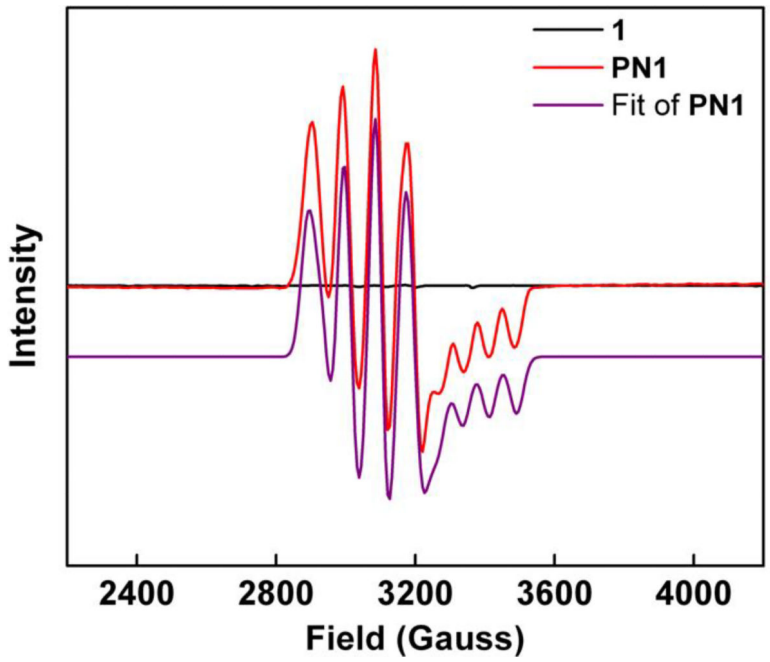

Figure 2.

X-band EPR spectra of **1** (black, EPR silent), **PN1** (red, 0.41 mM) and fitted **PN1** spectra (purple; $g_{1–3}$ = 1.9874, 2.1945, 2.2040; $A_{1–2}$ = 77.2 G, 111.3 G)

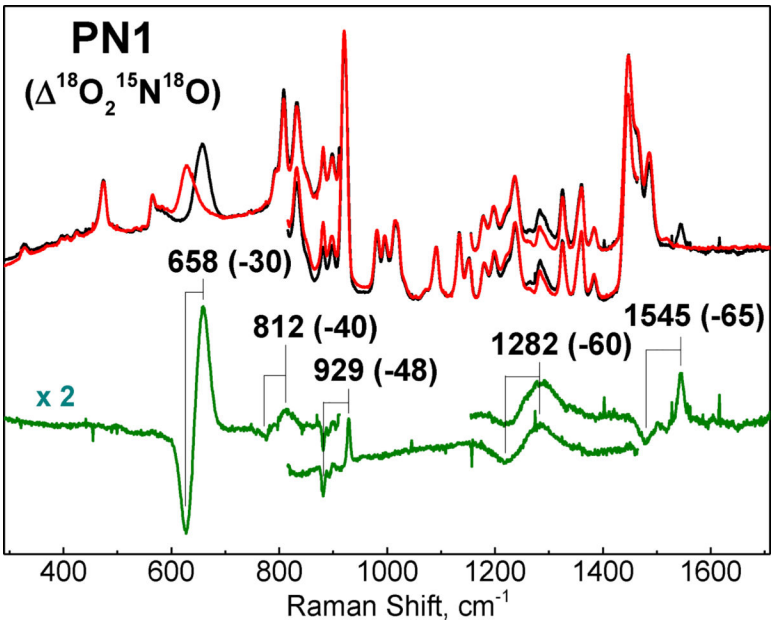

Figure 3.

RR spectra of **PN1** (407 nm excitation) generated from O_2 and $^{14}N^{16}O$ (black) or $^{18}O_2$, $^{15}N^{18}O$ (red). Difference spectrum (unlabeled – labeled) is shown in green.

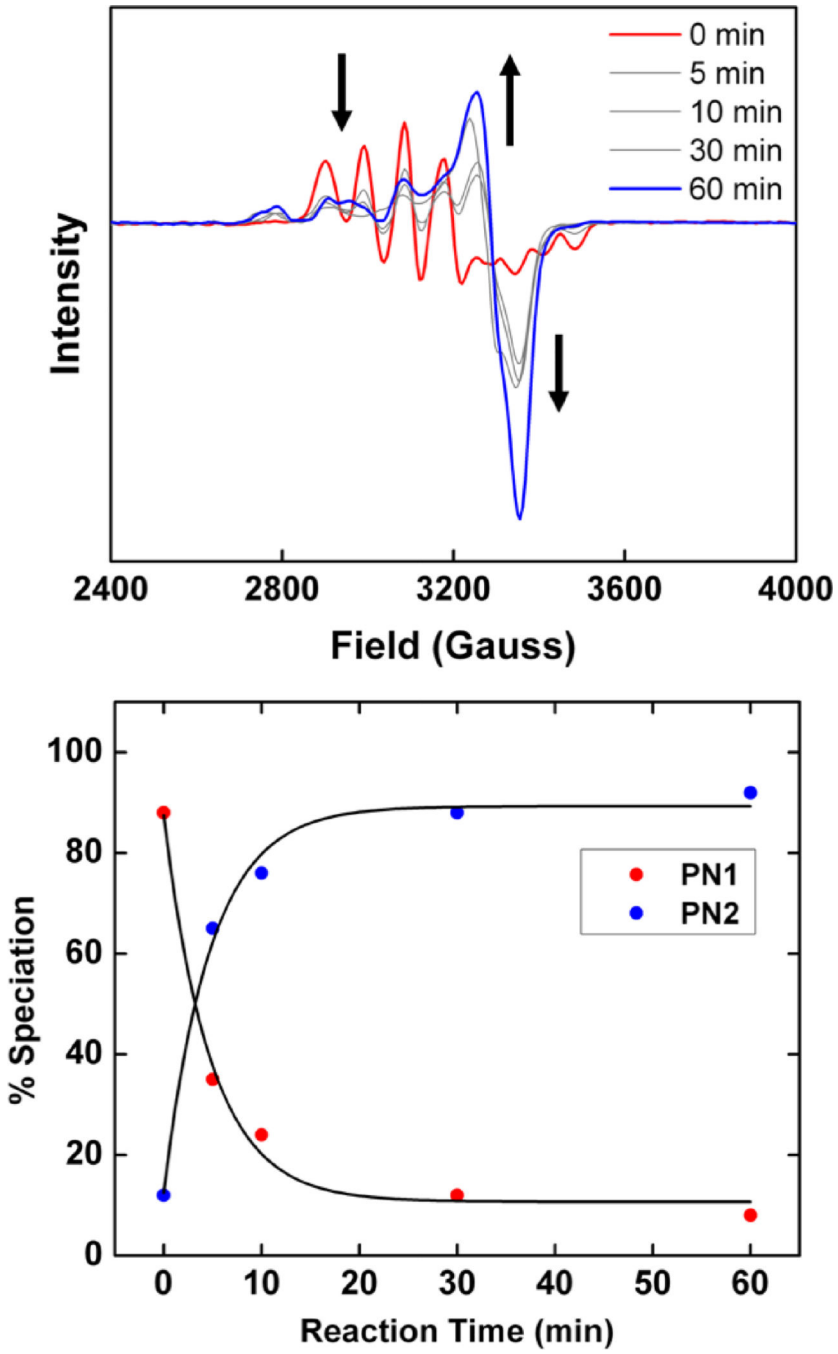

Figure 4.

(**Top**) Conversion of **PN1** (red) to **PN2** (blue) at –98 ºC (see Figure S10 for fitted EPR parameters of **PN2**). (**Bottom**) Speciation of **PN1** and **PN2** (calculated via EasySpin, Figure S27) as a function of time and fit to a single exponential. Conversion of 90% of **PN1** to **PN2** occurs within 30 minutes.

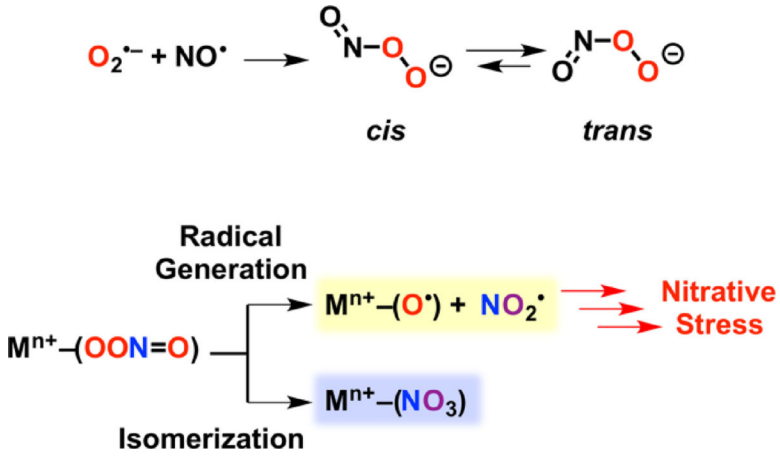

Scheme 1.

Formation of Peroxynitrite from Superoxide and Nitric Oxide, and Mechanisms of Peroxynitrite Decomposition through Metal Ion Coordination.

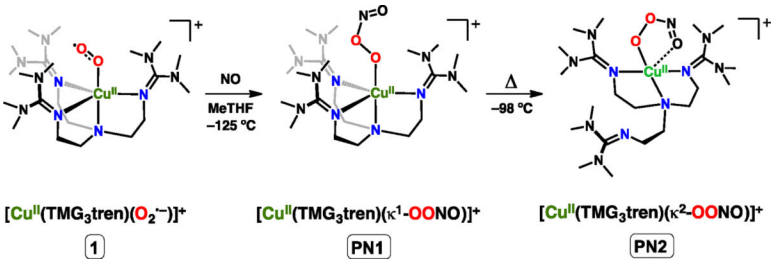

Scheme 2.

Generation of PN1 from addition of NO to complex **1**. Thermal transformation of **PN1** leads to formation of **PN2**.

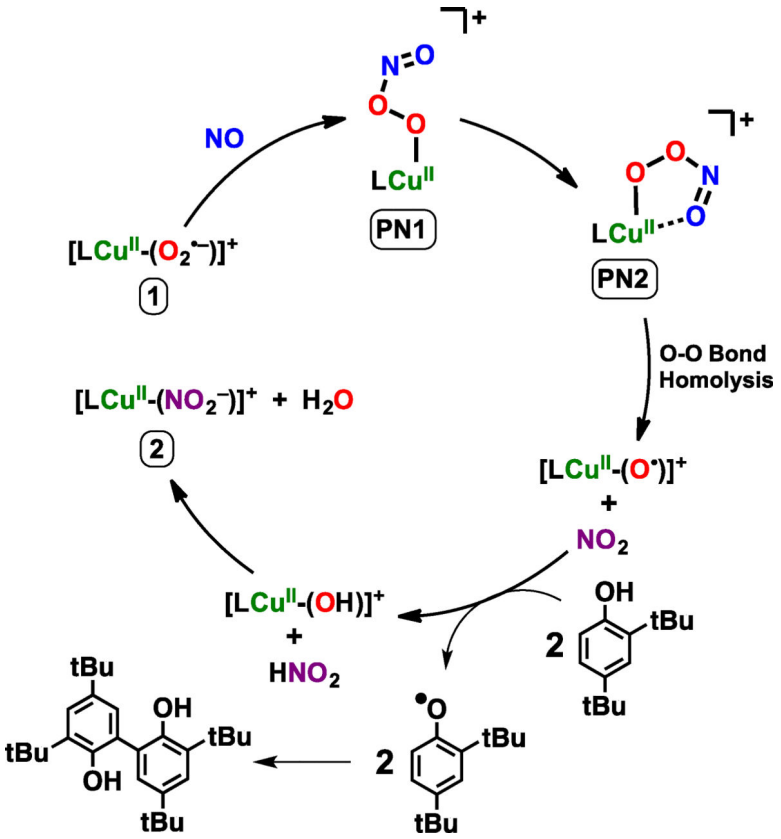

Scheme 3.

Proposed mechanism for 2,4-di-*tert*-butylphenol oxidation and Cu^{II}-NO_2^- production via **PN2** thermal transformation.

Table 1.

Summary of Isotopically Sensitive Vibrations of PN1; observed RR frequencies in cm^{-1} (isotope shift, cm^{-1}), and calculated frequencies for *cis* and *trans* conformers (italicized numbers).

Head 1	OONO	$^{18}O_2{}^{15}N^{18}O$	$^{18}O_2NO$	$OO^{15}N^{18}O$
ν(O–N) +δ(NO_2)	658	628 (−30)	637 (−21)	647 (−11)
cis	*708*	(*−35*)	(*−26*)	(*−9*)
trans	*845*	(*−45*)	(*−35*)	(*−12*)
ν(O–O) +δ(NO_2)	812	772 (−40)	---	---
cis	*833*	(*−45*)	(*−37*)	(*−14*)
trans	*630*	(*−35*)	(−23)	(−1*5*)
ν(O–O) +δ(NO_2)	929	881 (−48)	900 (−29)	912 (−17)
cis	*970*	(*−53*)	(*−35*)	(*−16*)
trans	*1002*	(*−51*)	(*−35*)	(*−15*)
ν(N=O)	1545	1480 (−65)	1543 (−2)	1482 (−43)
cis	*1601*	(*−68*)	(*−2*)	(*−68*)
trans	*1627*	(*−74*)	(*−3*)	(*−72*)